The atmospheric blocking influence over the South Brazil Bight during the 2013–2014 summer

Danilo A. Silva *, Marcelo Dottori

Oceanographic Institute, University of Sao Paulo, Praca do Oceanografico, 191, 05508-120 Sao Paulo, SP, Brazil

ARTICLE INFO

ABSTRACT

The 2013–2014 summer in the Southeast Brazil region set records for negative precipitation anomalies and the highest sea surface temperatures. Such event was attributed to the anomalous presence of atmospheric blocking, which prevented the propagation of a cold front towards the Equator and the establishment of the South Atlantic Convergence Zone, two phenomena that regulate the precipitation regime in this area. These blocking episodes are relatively important to the climate in mid-latitudes, but the feedback of the coastal ocean is still poorly understood under these anomalous conditions. This paper investigates, from a numerical perspective, the impacts on the thermohaline properties and circulation in the South Brazil Bight (SBB). We found that enhanced shortwave radiation leads to intense surface heating and that the presence of northeasterly winds strengthens the coastal upwelling nearby Cabo Frio. The South Atlantic Coastal Waters, transported into the SBB, regulate the extreme heating in the northern half of the domain, while, in the southern half, the absence of cold waters leads to the development of a warm-water pool. The final thermohaline structure induced an enlargement and intensification of the northwestward currents south of São Sebastião Island. Between Ubatuba and Cabo Frio, in the northern half, the northeasterly winds developed an intense surface advection towards offshore, and in the northern region, compensated by an opposite advection, towards the coast. We conclude that the coastal ocean feedback could present extreme anomalous conditions during atmospheric blocking events, leading to impacts upon the thermodynamical properties. Further studies are needed to understand the impacts of these events on biogeochemical properties.

© 2021 Elsevier B.V. All rights reserved.

1. Introduction

Atmospheric blocking, a large-scale, quasi-stationary weather phenomenon (Pinheiro et al., 2019), can strongly affect the upper ocean properties and circulation (Häkkinen et al., 2011), leading to the establishment of anomalous meteorological and oceanic conditions (Tibaldi and Molteni, 2018). During these events, mid-latitude westerly jet and synoptic scale transient weather systems might be interrupted or displaced during several days or weeks (Berrisford et al., 2007; Mendes et al., 2008). Their presence is associated with several extreme weather events, such as severe droughts (García-Herrera et al., 2007; Dong et al., 2018), striking heatwaves (Beniston, 2004; Chase et al., 2006), and flooding (Hong et al., 2011). Therefore, atmospheric blocking plays an important role in the mid-latitude weather variability (Sillmann and Croci-Maspoli, 2009; Woollings et al., 2018).

Blocking episodes occur more often in the southwestern Pacific (Lejenäs, 1984; Trenberth and Mo, 1985; Mendes et al., 2008), and with lower frequency in the western South Atlantic (Berrisford et al., 2007), persisting for 5 to 7 days. However, rare episodes can persist for more than 10 days, affecting several processes that regulate the local weather, such as the neighboring surface temperature and precipitation fields. Therefore, they have great potential to develop the aforementioned extreme weather events (Rodrigues and Woollings, 2017).

An example of this rare atmospheric condition is the extreme blocking event which occurred during the 2013–2014 summer in Southeast Brazil. During this period, the atmospheric blocking changed the wind regime in the region by blocking northeastward winds, associated with cold fronts (Fig. 1a to c). This high-pressure system also suppresses cloud formation. The result of that was extreme incoming shortwave radiation (Fig. 1d). In other words, this event drastically changed the ocean forcings and, consequently, the ocean conditions in the South Brazil Bight.

Despite the importance of atmospheric blocking to the climate in mid-latitudes, the feedback of the ocean is still poorly understood. The goal of this study is to examine the atmospheric blocking event of the 2013–2014 summer in further detail by assessing the impacts over the inner and middle shelves of the South Brazil Bight circulation and thermohaline properties.

* Corresponding author.
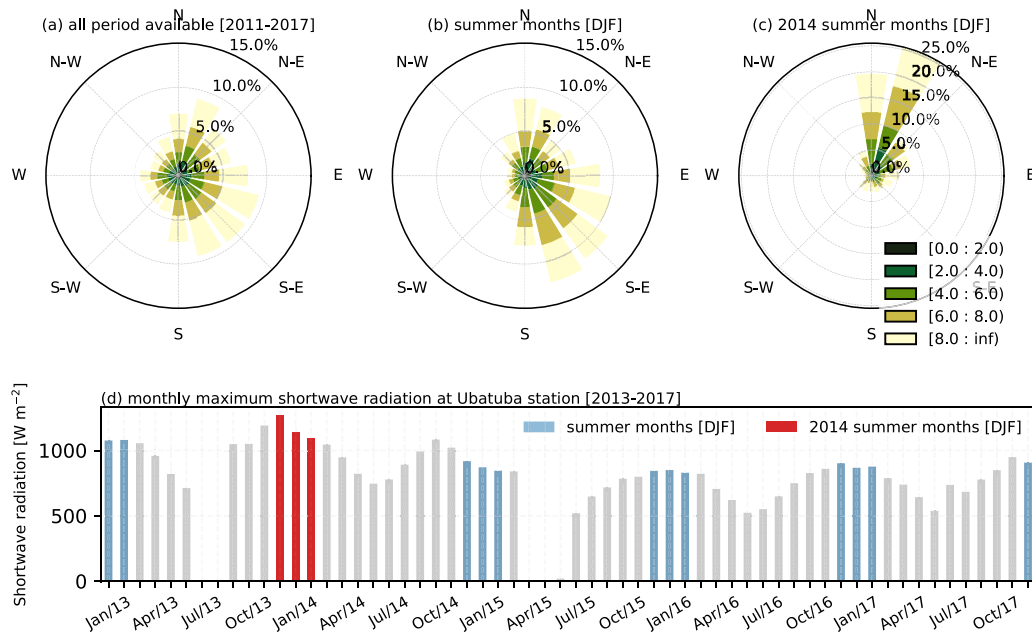 *E-mail address:* danilo2.silva@usp.br (D.A. Silva).

Fig. 1. The top panels present winds (meteorological convention) from the Buoy National Program (PNBOIA) at the South Brazil Bight from 2011 to 2017. Figure (a) shows the directional histogram of all data throughout the years, (b) only summer months in the same period, and (c) only 2013–2014 summer months. The colors indicate the intensity bands, varying from 0 to 10 m s^{-2}, and the distribution is in percentage. The directional histogram radial limits were kept different so it will be easier to observe the 2014 summer conditions relative to a typical summer. The lower panel (d) presents the histogram of the maximum monthly incoming solar radiation, from 2013 to 2017, observed in Ubatuba, at the meteorological station of the Oceanographic Institute of the University of São Paulo. The values are given in W m^{-2}, and colors highlight summer months (blue) and 2013–2014 summer months (red). (For interpretation of the references to color in this figure legend, the reader is referred to the web version of this article.)
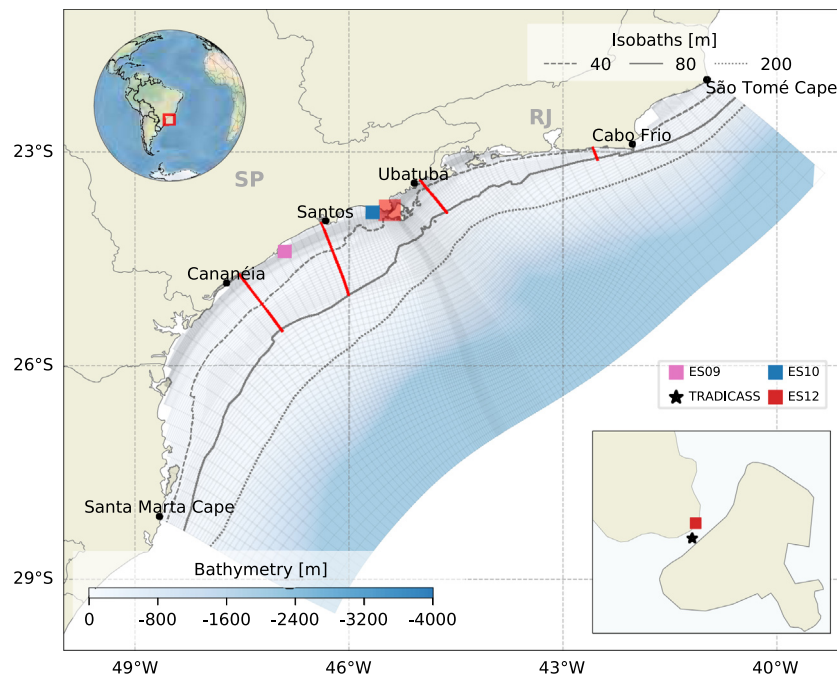

Fig. 2. Study area with full numerical domain (in light gray) and bathymetry (in meters) as colors. Three contours near the coastline identify the 40, 80 and 200 m isobaths and the four cross-shore red lines presents the transects used to discuss the numerical outputs. Markers on the map shows the location of each mooring used to validate the numerical model. The inset map highlights the São Sebastião Channel. (For interpretation of the references to color in this figure legend, the reader is referred to the web version of this article.)

1.1. The 2013–2014 summer event

In southern South America, blocking episodes prevent the equatorward propagation of cold fronts (Nieto-Ferreira et al., 2011), affecting the South Atlantic Convergence Zone (SACZ) establishment and, therefore, the precipitation regime. Due to the

subsidence activity, atmospheric blocking can also affect cloud cover, causing intensification of the incoming solar radiation and affecting the surface temperature field (Pfahl and Wernli, 2012).

During the 2013–2014 summer, the South Brazil Bight was under the influence of the most persistent event of atmospheric blocking ever registered in the area (Rodrigues and Woollings,

Table 1

Continental input used in both control (2006) and anomalous (2014) experiments, with average discharges obtained in the literature and reduced discharges computed based on the methodology described in Section 2.4.

	Cananéia [$m^3 s^{-1}$]		Santos [$m^3 s^{-1}$]	
	2006	2014	2006	2014
January	43	36.96	54	46.41
February	43	16.41	54	20.62

2017). Its persistence of almost 50 days resulted in relatively high values of air and sea surface temperature, as reported by Dottori et al. (2015), and a record negative precipitation anomaly (Coelho et al., 2016).

Some of the meteorological conditions during the 2014 summer are illustrated in Fig. 1. The wind regime was highly impacted, changing from winds varying from N/E/S (Fig. 1b) to winds blowing from N/NE (Fig. 1c). Remark that these two directional histograms have different radial axes limits to contrast the directional differences between a typical and anomalous event. Another major impact was the highest incoming solar radiation recorded in the Ubatuba (SP) meteorological station (Fig. 1d), during the 2014 summer months. During this summer, the highest maximum incoming solar radiation observed reached about 1200 W m^{-2}.

These extreme weather conditions led to the development of the worst drought episode faced by the Southeast Brazil metropolitan region (Nobre et al., 2016), culminating in the hydrical crisis of late 2015 that affected industries, tourism, recreation and food prices and energy fees, among other factors (Marengo et al., 2015).

1.2. The study region - SBB

The South Brazil Bight (SBB) is located in the southwestern South Atlantic (Fig. 2). It is a relatively wide shelf in the central region, with maximum width of 230 km, but it is narrow at its boundaries, ranging from 50–60 km (Castro, 2014) at Cabo Frio and Santa Marta Cape. The Brazil Current flows southward along the continental slope, transporting Tropical Water (TW) and South Atlantic Central Water (SACW) in the first 200 m of the water column (da Silveira et al., 2000). The first has temperature and salinity values higher than 20 °C and 36 psu, respectively, while the second has temperatures lower than 18 °C and salinities ranging between 35 and 36 psu. Coastal Water (CW), the third water mass of the SBB that occupies the nearshore zone, results from the mixing between TW, SACW, and low-salinity river-runoff waters (Castro and Miranda, 1998). Based on the characteristics of each water mass, the 18 °C-isotherm and the 36 psu isohaline are commonly used to identify the limits of the SACW and the TW, respectively.

The thermohaline structure of the SBB was used by Castro (1996) to separate the central sector of this continental shelf into three compartments: the inner, middle, and outer shelves. The synoptic wind regime and buoyancy advection, generated by the outflow of small rivers along the coast, dominate the inner shelf circulation (Castro, 2014; Morais, 2016). The resultant current flows northeastward, leaving the coastline to the left (Fontes and de Castro, 2017). The middle shelf exhibits a barotropic response to the wind regime, with the direction depending on that of the wind, both local (Dottori and Castro, 2009) and remote (Dottori and Castro, 2018). The outer shelf circulation is primarily driven by the BC and, to a weaker degree, by the synoptic wind (Castro et al., 2008).

The wind regime in the SBB is produced by two meteorological systems: the large-scale South Atlantic Subtropical High

(SASH) and the passage of meso-scale cold front systems (Castro and Miranda, 1998). The first corresponds to a more persistent system, blowing from East-Northeast, and the second presents an intermittent characteristic, with a synoptic frequency of 6 to 11 days, blowing from south/southwest (Stech et al., 1992). The cold front systems, with synoptic scales, are associated with heavy rainfall in southern Brazil (Teixeira and Satyamurty, 2007) and, when combined with the South Atlantic Convergence Zone (SACZ), regulate the precipitation regime in the region.

2. Materials and methods

In this study, we use an implementation of the Estuarine, Coastal and Ocean Model, called ECOM, (Blumberg and Mellor, 1987) for the South Brazil Bight. The model description and its setup are provided in Section 2.1 and follow a similar configuration as in Costa et al. (2019). We select the simulation periods based on the methods detailed in Section 2.2 and described in Sections 2.3 and 2.4. Finally, we validate the model by performing quantitative and qualitative approaches, based on in situ observations and remotely sensed sea surface temperature, respectively (Section 2.5).

2.1. Model setup

The model used in this study is an implementation of the Estuarine, Coastal and Ocean Model (ECOM) (Blumberg and Mellor, 1987) to the South Brazil Bight. The hydrodynamic module uses the finite difference method to solve the primitive equations, under the hydrostatic assumption and Boussinesq approximation, to compute prognostics of sea surface elevation and 3D fields of currents, temperature and salinity. The model also includes a second-order turbulence closure model (Mellor and Yamada, 1982) and the Smagorinsky (1963) formulation to parameterize the vertical and horizontal mixing processes.

The numerical domain (Fig. 2), adapted from Pereira et al. (2007) to fit with the available climatological information, is an orthogonal, curvilinear Arakawa C-grid with sigma vertical coordinates. It covers the South Brazil Bight from Santa Marta Cape to São Tomé Cape, and is designed to present a higher resolution in the São Sebastião Channel (inset map in Fig. 2), at the central region of the study area. Therefore, the alongshore direction has 110 grid cells, decreasing the resolution from 0.5 km, at the center, to 35 km, towards the open boundary. In the cross-shore direction, there is a total of 137 grid cells, varying from 0.2 km, in the inner continental shelf, to 35 km in the deep ocean area. The depth varies from 5 to 2.000 m in 21 equally spaced sigma levels. The vertical resolution was chosen in order to reduce the artificial pressure gradient error generated by the steep topography. Pereira et al. (2007) shows that for this same numerical grid, 24 sigma levels generates an alongshore geostrophic flow error of 0.5–1.5 mm s^{-1}, which is much lower than the alongshore currents observed in the SBB.

As initial conditions, we warmed the model with a 12-day spin-up run, forced only by three-dimensional summer climatological fields of temperature and salinity. This climatology presents the main thermohaline patterns in the study area, like the coastal upwelling near Cabo Frio, the low-temperature waters coming from the Rio de la Plata, and the low-salinities strip nearshore, resulted from several small rivers along the coast (Costa et al., 2019). Rezende (2003) show that a 12-days spin-up is enough to warm up the SBB, reproducing patterns like the Brazil Current flowing southward at the shelfbreak, and northeastward currents nearshore, corroborating with the main current patterns in the SBB (Castro, 1996; Dottori and Castro, 2009; Costa et al., 2019). The open boundary condition was set
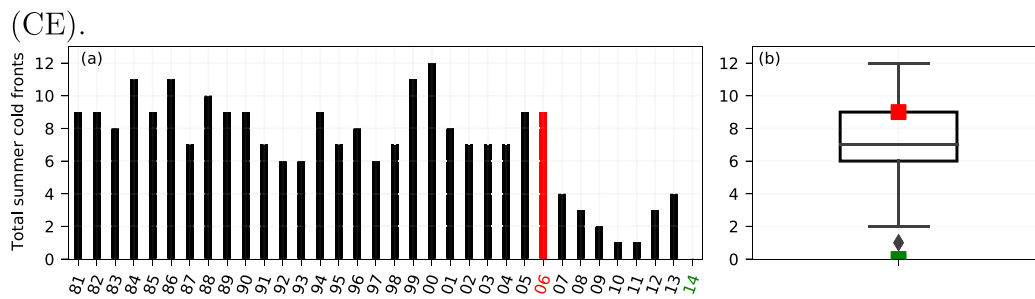
(CE).

Fig. 3. Cold front occurrences during summer months from 1981 to 2014 (a) and boxplot summarizing statistical parameters computed with this time series (b). In both figures, colors highlight the 2006 (red) and 2014 (green) summers. (For interpretation of the references to color in this figure legend, the reader is referred to the web version of this article.)
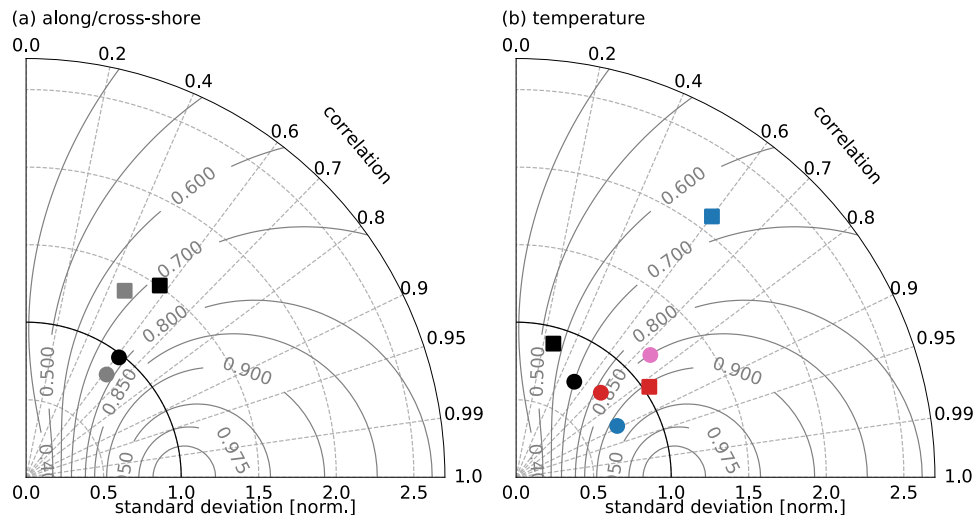

Fig. 4. Taylor's diagram for (a) cross (gray) and alongshore (black) current components and (b) for seawater temperature. In this figure (b), each color represent a location showed in Fig. 2. The markers represent vertical levels of observations: circle for near surface and squares for near bottom. The skill score is indicated as gray continuous contour lines on the diagram. The period used to compute these statistics goes from January 14th to March 1st of 2014 and all values are statistically significant, above the 95% confidence level, using the method of Ebisuzaki (1997). (For interpretation of the references to color in this figure legend, the reader is referred to the web version of this article.)

as radiative using the formulation proposed by Reid and Bodine (1968), which allows the energy crossing in both directions at the boundaries. Since the main focus of this domain are the São Paulo and Rio de Janeiro continental shelves, a broader numerical grid was chosen to reduce the propagation of numerical errors from the boundaries. Additionally, we prescribed temperature and salinity climatologies at the open boundaries. The time steps used to solve the internal and external modes were 10 s and 1 s, respectively. All experiments were conducted in the prognostic mode, which enables the development of the thermohaline structure during the simulations.

More details about this particular ECOM setup and the SBB model grid can be found in Costa et al. (2019).

2.2. Summer selection

Two experiments were carried out in this study. One of them consists of a control experiment, a summer with an average amount of cold fronts occurrences (CE from now on), and another covering the 2013–2014 summer (Anomalous Experiment or AE). Since the atypical period of 2014 was characterized by the absence of frontal systems, we used the number of cold fronts during the summer as the criterion to choose the period classified as the control/typical summer. This selection was made based on the occurrences of cold fronts in the Southeast Brazil region during summer extracted from two different datasets. From 1981

to 2002, we obtained cold front occurrences from Dametto and Rocha (2006), and from 1996 to 2014, we extracted this information from the Climanalise Bulletin, available at http://climanalise.cptec.inpe.br/~rclimanl/boletim/. The coincident period between these two datasets presents differences of no more than one cold front in a month, and thus we combine them. With 34 years of cold front occurrences during summer months, from 1981 to 2014, we used basic statistical (mean and standard deviation) parameters to select the average summer. Given these criteria, we select the 2006 summer, which included a total of 9 cold front passages.

We integrated the model from January 9th to March 1st of 2006 (CE) and 2014 (AE). However, we only analyzed the outputs between January 13th and February 14th, considering the period of the most persistent blocking event detected in the Southeast Brazil region (Rodrigues and Woollings, 2017). During this period, notable observations include an absence of southwesterly winds and cloud cover, anomalous negative precipitation rates, and positive anomalies with respect to incoming solar radiation, as already described. Once again, the simulations depart from a dynamical condition established by the spin-up.

2.3. Atmospheric input

Due to its superior performance in representing extreme events (Stopa and Cheung, 2014), we prescribed surface meteorological fields of wind and heat fluxes from CFSR (Saha et al.,
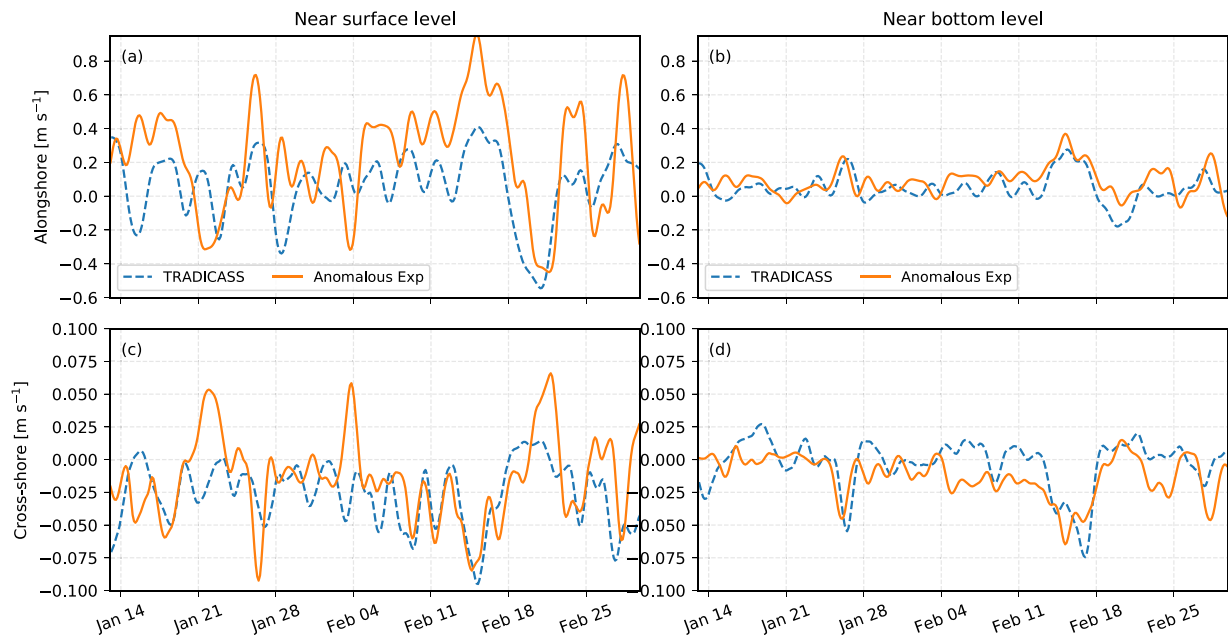
Fig. 5. Low pass filtered time series of alongshore (top panels) and cross-shore (lower panels) current components in m s^{-1}. Dashed line are for observed data and the continuous lines represent modeled products. The period presented includes January 14th to March 1st of 2014.
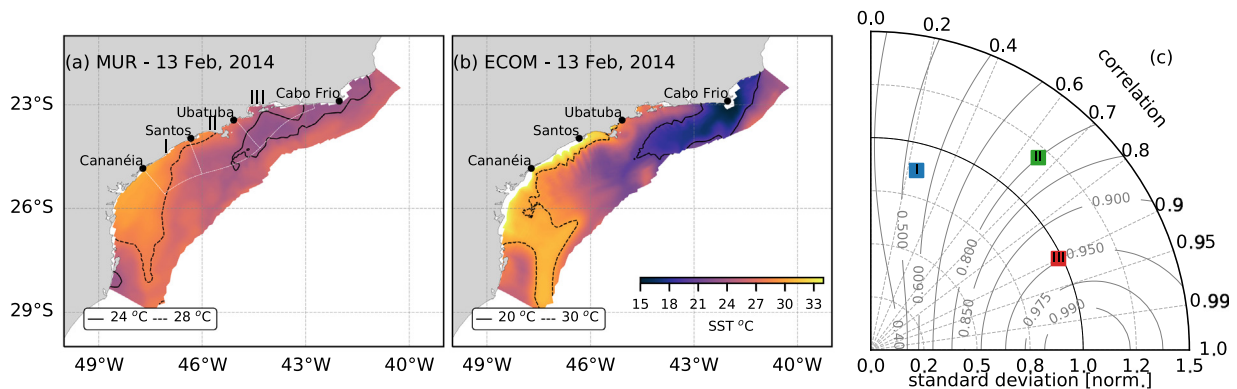

Fig. 6. Maps of qualitative comparison between sea surface temperature from (a) Level 4 Multiscale Ultrahigh-Resolution (MUR) and (b) output from the Anomalous Experiment for February 13th of 2014. The white contour inside (a) stands for the sectors used to compute a box-averaged daily time series used to produce the statistical parameters on the diagram (c): the blue square is related to the southernmost area (Cananéia and Santos), the green square is the central area (Santos and Ubatuba), and the red square is the northernmost area (Ubatuba and Cabo Frio). The skill score is indicated as gray continuous contour lines on the diagram and all values are statistically significant, above the 95% confidence level, using the method of Ebisuzaki (1997). Data from MUR were extracted from the Physical Oceanography Distributed Active Archive Center (PODAAC), found in http://podaac.jpl.nasa.gov/. (For interpretation of the references to color in this figure legend, the reader is referred to the web version of this article.)

2010) and CSFv2 (Saha et al., 2014) reanalysis database, provided by NCEP/NCAR, to force the exchange of momentum and heat between the atmosphere and the ocean.

The 10-m wind components were used to compute wind shear at the surface of the ocean, with a classical quadratic parameterization, calculating the drag coefficient based on the wind intensity, as proposed by Large and Pond (1981). We compute the net heat flux (Q_{net}) based on the following equation:

$$Q_{net} = Q_{SW} + Q_{LW} + Q_h + Q_e \qquad (1)$$

where Q_{SW} is shortwave radiation flux, Q_{LW} is the longwave radiation flux, Q_h is the sensible heat flux and Q_e is the latent heat flux, all of which are extracted from the reanalysis dataset. Both forms of meteorological data were interpolated on the SBB grid, retaining the 6-hourly frequency resolution.

2.4. Continental input

Freshwater inputs were specified at two locations, representing the major estuarine systems in the SBB: Santos and Cananéia (indicated in Fig. 2). The first, located in the central area of the numerical domain, has an average discharge of 54 m^3 s^{-1} during typical summer conditions, computed from the values presented by Roversi et al. (2016), while the second, in the south, contributes mean values of 43 m^3 s^{-1} (Bonetti Filho and de Miranda, 1997).

Due to the lack of flow monitoring in the Santos and Cananeia estuarine system, reduced discharges had to be estimated to represent a decrease in the flow associated with the drought during the summer of 2014. Monthly climatological precipitation rates (P_{clim}) for January (231.3 mm) and February (215.2 mm) were used to compute the reduced river discharge. These values were extracted from the Quarterly Climatological Bulletin for DJF 2013/2014 of the Institute of Astronomy, Geophysics and
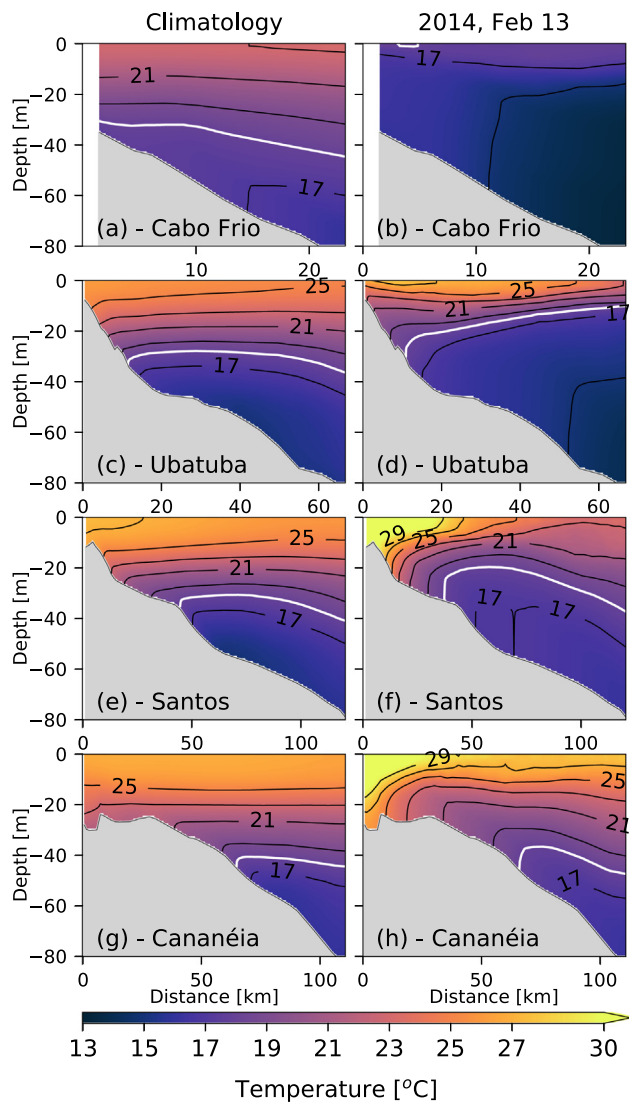
Fig. 7. Transect of temperature off Cabo Frio (a and b), Ubatuba (c and d), Santos (e and f) and Cananéia (g and h). The left column presents the summer climatology for each transect, used to initialize the simulations, and the right column provides the daily mean for February 13th of 2014. The white line represent the 18 °C-isotherm.

Atmospheric Sciences of the University of São Paulo, accessed at http://www.estacao.iag.usp.br/Boletins/DJF20132014.pdf. We then combine the average estuarine discharges ($\overline{Q_f}$) and the monthly precipitation rates (P^{2014}) for January 2014 (199.3 mm) and February 2014 (81.1 mm) to estimate the reduced estuarine discharges (Q_f^{2014}) during January and February 2014 using the following:

$$Q_f^{2014} = \frac{\overline{Q_f}\, P^{2014}}{P_{clim}} \qquad (2)$$

The values used in each simulation are summarized in Table 1.

2.5. Model performance

To ensure the performance of the model, we used several moorings with current meters and temperature sensors, distributed in the central area of the numerical domain (Fig. 2). All dataset were corrected for the magnetic declination, using the nearest coastline orientation to decompose vectors to along

and cross-shore components and then low-pass filtered using a Lanczos square filter (Duchon, 1979), with a cutoff frequency of 40 h to remove inertial and tidal frequency oscillations. The observed time series was used to compute the Pearson Coefficient Correlation (R, henceforward), the root mean square error (RMSE) and the Skill Score proposed by Willmott (1981).

The observational data used came from two projects conducted by the Oceanographic Institute of the University of São Paulo. The ECOSAN project (squared markers in Fig. 2), collected data during 2005 and 2006. Therefore, we validate the CE seawater temperature output. The other project, called TRADICASS (star marker in Fig. 2), is a long-term effort to monitor the seawater physical properties in the middle of the São Sebastião Channel (SSC). From this dataset, we used observations for the 2014 summer, validating the currents and seawater temperature from the AE results.

We also used Level 4 SST extracted from the Multiscale Ultrahigh-Resolution (MUR) dataset (Chin et al., 2017) for comparison with the modeled SST. This dataset provides daily gridded SST with 1-km spatial resolution, available in the Physical Oceanography Distributed Active Archive Center (PODAAC–http://podaac.jpl.nasa.gov/).

3. Results

3.1. Cold front distribution

The number of cold fronts obtained from the Climanalise Bulletin and Dametto and Rocha (2006) are presented in Fig. 3. The results show a relatively regular cycle from 1981 to 2006. After this period, from 2007 to 2014, there is a substantial decrease in the number of cold front systems, with extreme cases in 2010 (1), 2011 (1) and 2014 (0). On average, there are 7 ± 3 cold fronts in total per summer. From this same dataset, the 2006 summer exhibited a total of 9 cold front occurrences, within the upper quartile (Fig. 3b) and was also the last summer before the abrupt decrease of occurrences. Therefore, we use this year as the typical summer in the control experiment (CE).

3.2. Model evaluation

The quantitative assessment focused on the ability of the model to reproduce the alongshore and cross-shore current components and the temperature in several locations (indicated in Fig. 2). Near the surface, the alongshore (cross-shore) component (Fig. 4a) shows skill of 0.65 (0.65), correlation of 0.57 (0.48) and RMSE of 0.09 (0.01) m s^{-1}. The best statistical values were found near the bottom, with the alongshore (cross-shore) component presenting a skill of 0.73 (0.73), a correlation of 0.61 (0.60) and RMSE of 0.07 (< 0.01) m s^{-1}. This good agreement between the EA output and the observations are presented in Fig. 5. Regarding the seawater temperature (Fig. 4b), we found skill values ranging from 0.6 to 0.9, correlation coefficients between 0.4 and 0.9.

We quantitatively compared SST from remotely-sensed products (MUR) with the Anomalous experiment output (Fig. 6a and b), that exhibited good agreement, presenting the main features in the South Brazil Bight domain. To quantify this assessment, we extract a box-averaged daily time series for both datasets in three sectors between the transects (white contour in Fig. 6a): (I) between Cananéia and Santos, (II) between Santos and Ubatuba, and (III) between Ubatuba and Cabo Frio. The statistics between these time series (Fig. 6c) presents correlation coefficients of 0.25, 0.72 and 0.9 for the sectors I, II and III respectively.
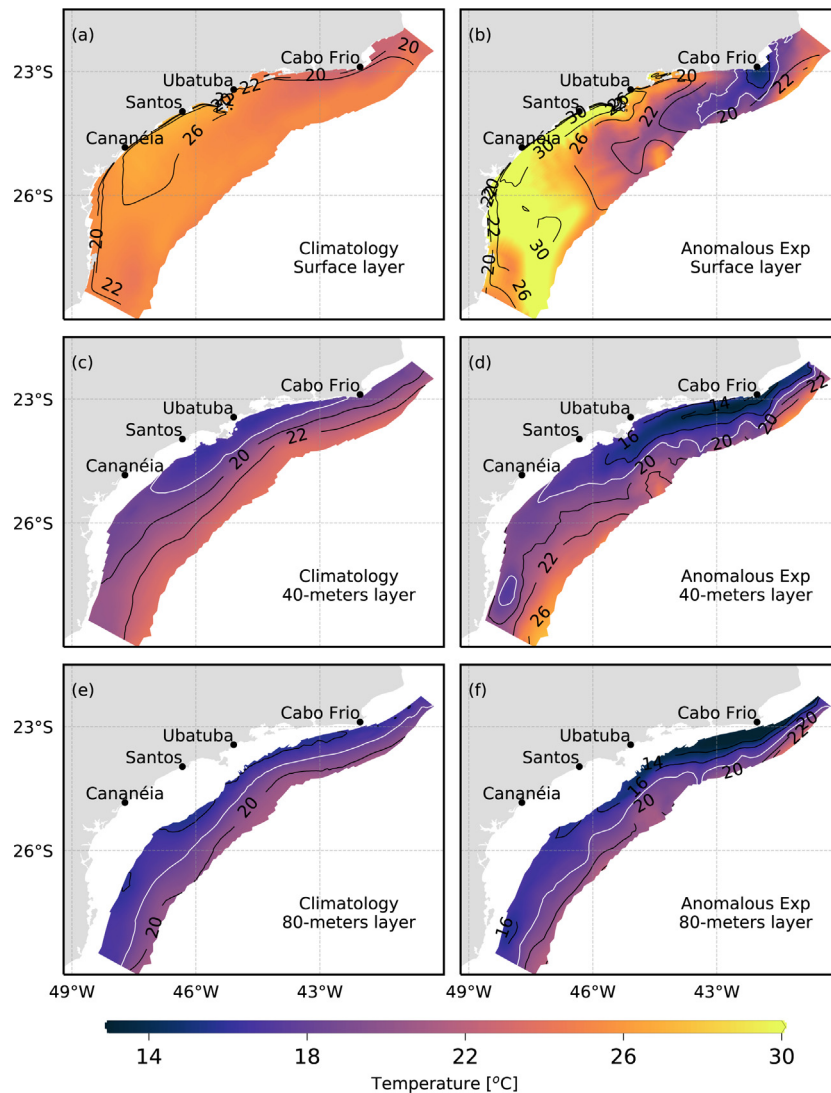
Fig. 8. Horizontal distribution of temperature for the surface (a and b), 40-m depth (c and d) and 80-m depth (e and f). The left column presents the summer climatology in each layer, and the right column provides the daily mean for February 13th of 2014. The white line represent the 18 °C-isotherm.

3.3. The thermohaline structure

The description of the anomalous thermohaline structure is achieved by comparing temperature and salinity model outputs of February 13th with the summer climatological data, using the 18 °C-isotherm and the 36 psu isohaline as proxies for the SACW and TW displacement, respectively.

The vertical distribution of SACW and TW is assessed by the analysis of four transects distributed along the SBB off Cananéia, Santos, Ubatuba and Cabo Frio (Fig. 2). Additionally, the horizontal distributions of temperature and salinity are presented in three vertical layers: at the surface, 40 m deep and 80 m deep.

In Cabo Frio (Fig. 7, a and b), there is an intense prevalence of waters colder than 18 ^{o}C, both for climatological and anomalous conditions. However, at the end of the anomalous period, the entire shelf is filled with SACW, delimited by the 18 °C-isotherm, including the surface. Off Ubatuba (Fig. 7, c and d), the 18 ^{o}C-isotherm rises considerably, mainly offshore. However, this region is more stratified than the previous transect. In this section, warmed waters occupy the first 10 meters near the surface, but with values which remain colder than the climatology.

Off Santos (Fig. 7.e and f), there is a slight 18 ^{o}C-isotherm uplift, reaching regions shallower than 20 m between 50 and 70 km offshore. Due to the influence of subsurface cold waters, the surface temperatures are lower than the climatology near the 60-m isobath and approximately 100-km offshore, decreasing from 24 ^{o}C to 22 ^{o}C when compared to the climatology. The most prominent feature, however, is observed near the coast, with temperatures reaching anomalous values higher than 30 ^{o}C.

Off Cananéia (Fig. 7, g and h), we observe small variations of the 18 ^{o}C-isotherm position, warmer surface waters along the transect, and extreme heating of the entire water column from the coast up to 30-km offshore, with temperatures higher than 30 ^{o}C, similar to the Santos transect. The pattern found in this transect suggest an advance of cold offshore waters near the bottom that is balanced by the anomalous heating of surface waters, resulting in smaller variations.

The sea surface temperature distribution (Fig. 8.a and b) shows an intensification of coastal upwelling, with a cold water core near Cabo Frio that was advected into the SBB, mainly in the middle shelf (between the 40-m and the 80-m isobaths). SST varies between 17 ^{o}C and 20 ^{o}C in the northern region. In the south, however, warm waters dominate the temperature field, from the coast to the shelf break, with values higher than 29 ^{o}C.

The temperature distribution 40 m deep (Fig. 8.c and d) shows this increase in the upwelling, as well as the intrusion of cold
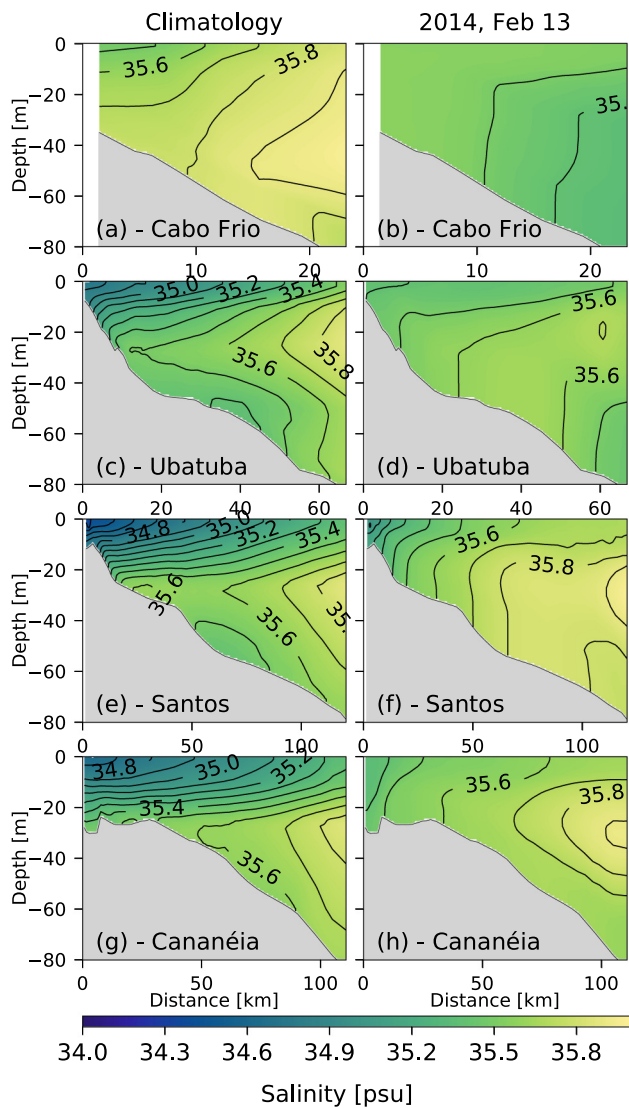
Fig. 9. Transect of salinity off Cabo Frio (a and b), Ubatuba (c and d), Santos (e and f) and Cananéia (g and h). The left column presents the summer climatology for each transect, used to initialize the simulations, and the right column provides the daily mean for February 13th of 2014. The white line represent the 36 psu isohaline.

waters by both cross and alongshore advection. Finally, in the 80-m deep layer (Fig. 8.e and f), colder waters than the climatology are presented in the northern region of the domain, with almost no distribution change in the southern portion.

Regarding the salinity, an intense homogenization occurs off Cabo Frio (Fig. 9, a and b), with lower than climatological salinity waters covering the entire transect, varying from 35.3 to 35.4 psu. Off Ubatuba, Santos, and Cananéia (Fig. 9, c and d, e and f, g and h, respectively), there is a weakening of the vertical salt gradient, but with a broader range of horizontal variation, from 35.4 to 35.8 psu, while climatologically, salinity varies from 34.8 to 35.8 psu due to the runoff discharge influence in those areas. The isohalines suggest an advection of water towards the coast, while at the surface this transport occurs in the opposite direction. This appears to be evident in the 35.6 psu isohaline pattern, mainly in the Ubatuba and Santos transects.

At the surface, saltier waters fill the inner shelf, increasing salinity from the climatological value of 34.5 to 35.5 psu, mostly between Cananéia and Santos. For the entire middle shelf, salinity

changes from 34.8 to values higher than 35.5 psu at the surface (Fig. 10, a and b). Even with this increase, the 36 psu isohaline moved to deeper regions, reaching the 1000-m isobath in some areas, and decreasing the horizontal salinity gradient. This displacement is also observed at 40 m and 80 m depth layers (Fig. 10, c and d, d and f, respectively), but mainly in the northern area. In both layers, we observe a decrease in the salinities surrounding Cabo Frio, with values decreasing from 36 to lower than 35.5 psu. In the rest of the domain, however, no pronounced changes were found.

3.4. Circulation

We decomposed the currents into alongshore and cross-shore components. Positive values indicate an offshore flow for the cross-shore component (Fig. 12, left) and northeasterly flow for the alongshore component (Fig. 12, right).

In general, there is a northeastward current intensification over the inner shelf from the coastline to the 40-m isobath. In this region, current intensities higher than 0.2 m s^{-1} occurred on February 13th (Fig. 11a and b). South of São Sebastião Island (SSI), we can also identify an enlargement of the northeastward currents reaching the 80-m isobath. In the northern region, however, the inner and middle shelf surface current response tends to transport waters towards offshore, characterized by surface currents almost perpendicular to the coastline (southeastward). Despite the intensification of the currents, the 40-m depth layer (Fig. 11c and d) exhibited small variations on February 13th compared with the average circulation in the control experiment. At the 80-m depth layer (Fig. 11e and f), however, the northern region presents currents towards the coast, transporting waters from the shelfbreak to shallower regions, compensating for the surface offshore transport.

In terms of vertical structure, off Cabo Frio there is cross-shore component towards offshore (Fig. 12a), with current magnitudes higher than 0.2 m s^{-1} in the first 20 m of the water column. The alongshore component (Fig. 12b), however, is dominated by positive magnitudes, between 0.2 and 0.3 m s^{-1}, which indicates northeastward currents in this area. Off Ubatuba a similar pattern were observed for the cross-shore component (Fig. 12c), but the alongshore is dominated by negative values (southwestward) (Fig. 12d).

For Santos and Cananéia, cross-shore components (Fig. 12e and g) towards offshore dominate both transects, with magnitudes of 0.2 m s^{-1} located from the coastline to approximately 70 km offshore. In addition, the northeastward alongshore component (Fig. 12f and h) dominates from the coast to the 20-m isobath, with higher intensities confined near the coast. From the 20-m isobath, there is a reversion of the alongshore component, presenting mild and negative values (southeastward).

In respect to the cross-shelf currents – currents decomposed using the orientation of the 80-m isobath along the continental shelf – (Fig. 13), we observed a general intensification. Offshore currents of 0.3 m s^{-1} on average dominate the surface levels, but with extreme and deeper offshore currents in two main regions: south of São Sebastião Island, where offshore currents dominate all the water column, and west of Cabo Frio.

From 10 m to the bottom, onshore cross-shelf components dominate the section, except between 180–280 km from the coast, varying between 0.01 and 0.03 m s^{-1}, with extreme values higher than 0.06 m s^{-1} concentrated in a single well-defined core. Relative to the average CE condition (Fig. 13a), this formation suffers an enlargement and deepening, changing from about 100-km wide and 40-m thick up to 200-km and 70-m, respectively. There is no well-defined organization for the onshore currents between 0 and 150-km.
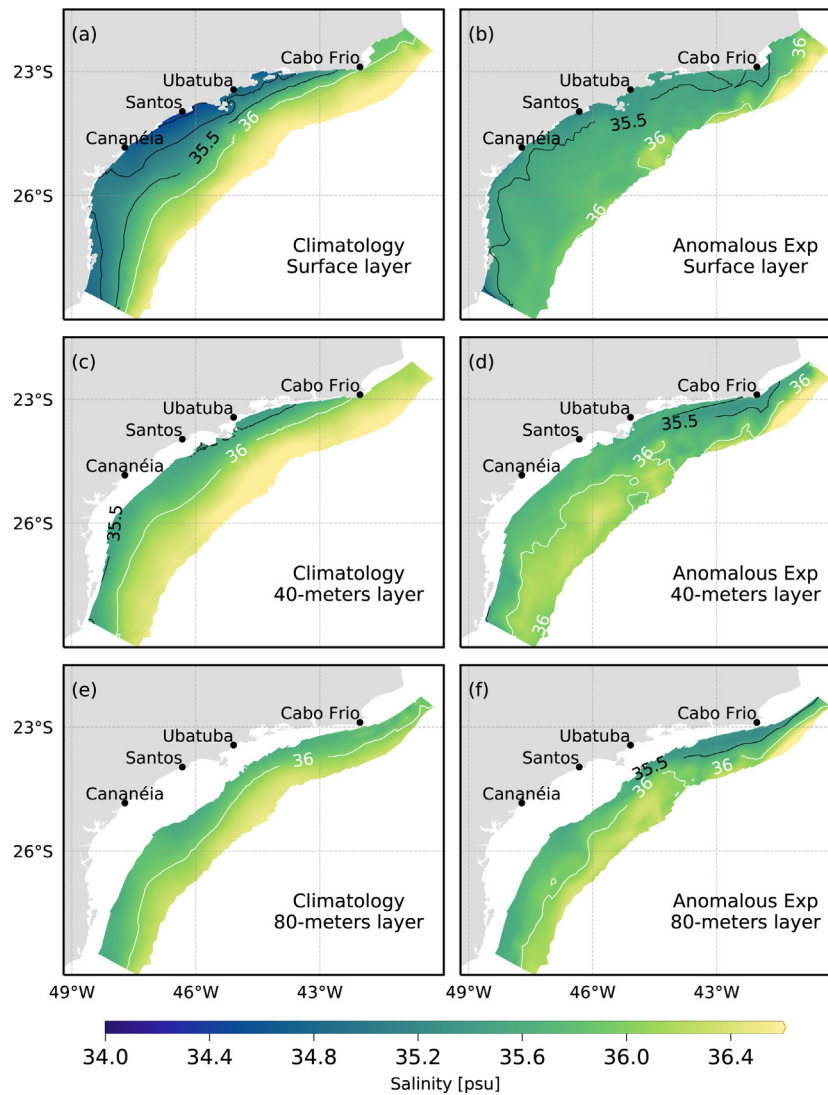
Fig. 10. Horizontal distribution of salinity for the surface (a and b), 40-m depth (c and d) and 80-m depth (e and f). The left column presents the summer climatology in each layer, and the right column provides the daily mean for February 13th of 2014. The white line represent the 36 psu isohaline.

4. Discussion

The quantitative assessment shows that the model exhibited good agreement with the alongshore component (Fig. 4.a), with better results found near the bottom. These results suggest that the model properly reproduces the hydrodynamical response to the main processes that drive the circulation, such as winds and thermohaline forcings (Castro, 1990). Since the São Sebastião Channel dynamics is highly driven by the adjacent continental shelf dynamics (Castro, 1996; Dottori and Castro, 2009; Dottori et al., 2015; Dottori and Castro, 2018), we can extend this assessment for the inner and mid-shelves, the main region of analysis in this work.

The temperature comparison (Fig. 4.b) presents better results near the bottom than the surface, mainly because of the processes that control this variable at each vertical level. At the bottom, horizontal advection of cold water dominates the temperature variability in the summer (Cerda and Castro, 2014), while heat fluxes in the air-sea interface near the surface seem to be the main mechanism that controls the SST. However, the heat flux dataset used in this work is susceptible to biases caused by the parameterization process (Zeng et al., 1998; Josey, 2001). The correlations between modeled and observed temperatures

are comparable with similar studies that evaluate the performance of hydrodynamic models in continental shelf regions, such as Zhang et al. (2012) and Hetland and DiMarco (2012) for the Texas-Louisiana continental shelf circulation and temperature.

The SST assessment (Fig. 6a and b) shows lower values in the northern region, with an offset of approximately 5 °C. This offset is discussed by Pereira et al. (2020), indicating that Level 4 SST MUR products exhibit discrepancies when confronted with in situ observations, with higher differences observed during upwelling days. Even with the bias inserted into the model by the heat flux dataset used, as discussed above, the absence of a two-way air-sea exchange configuration in the model can explain the higher SST values observed in the southern region. Despite that, qualitatively the main mesoscale features are well represented in the simulation, showing an extension of cold waters plume from Cabo Frio to Ubatuba and the warm-water pool, in the southern region, with higher SST. The box-averaged SST correlation coefficients (Fig. 6c) computed are quite acceptable for the upwelling and the central zones (R of 0.9 and 0.7, respectively). The low correlation in the warm-water pool (R of 0.24) might be associated to the fact that it was not possible to reproduce the transition zone position appropriately, relative to the MUR product. While in our results
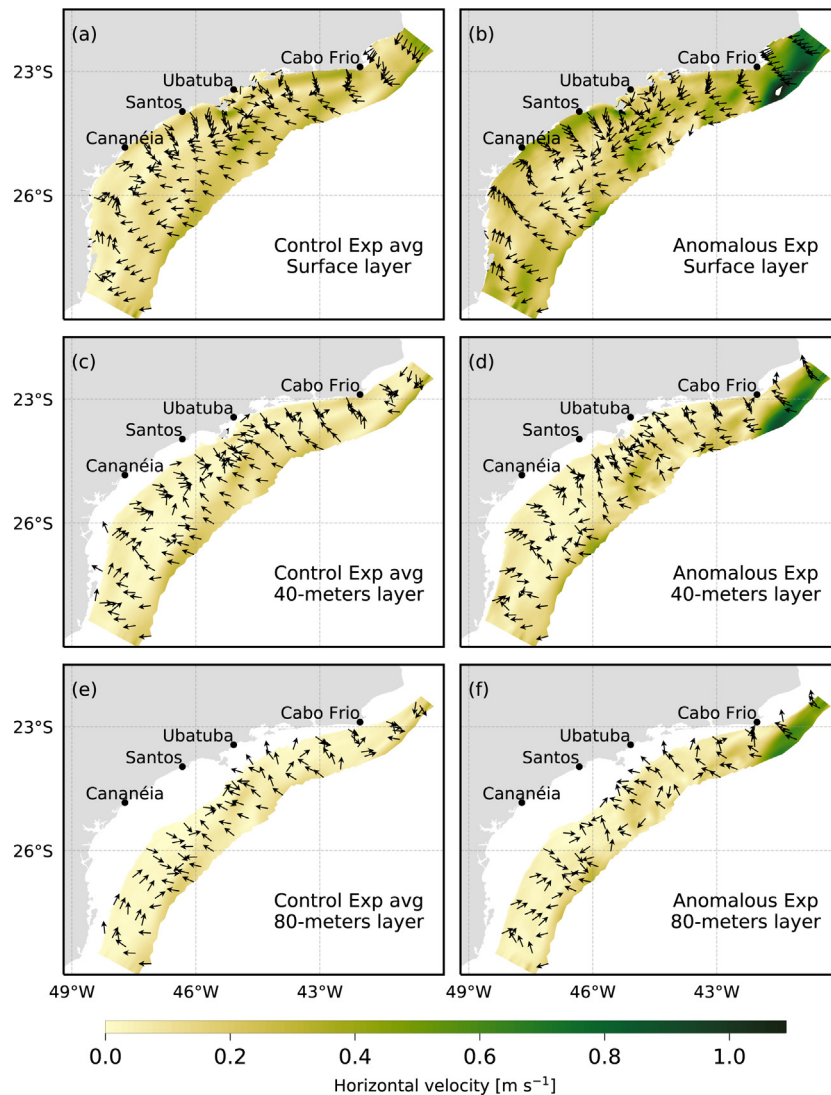
Fig. 11. Horizontal distribution of velocity for the surface (a and b), 40-m depth (c and d) and 80-m depth (e and f). The left column presents the average circulation in the Control Experiment for each layer, and the right column provides the daily mean for February 13th of 2014.

the transition zone is oriented in the along shelf direction (30 °C-isotherm in Fig. 4b), in the remotely-sensed SST we observed a north-south oriented transition zone (28 °C-isotherm in Fig. 4.a).

4.1. Thermal blocking and TW displacement

At the SBB, northeasterly winds are well known as upwelling-favorable (Emilsson, 1961; Ikeda, 1977). In the northern SBB region, the narrow shelf enhances this dynamical process, resulting in the coastal upwelling around Cabo Frio (Valentin, 2001). The northeasterly winds persistence for more than 30 days in 2014 caused a coastal upwelling intensification (Fig. 6). The cold waters plume reach regions further south than the climatological limits, transported by the Brazil Current and southwestward currents at the mid-continental shelf surface levels.

Off Ubatuba, we do not observe a classical coastal upwelling as expected due to a narrow shelf in this area. Instead, an 18 °C-isotherm uplift takes place, suggesting that the near-bottom on-shore cold waters advection was thermally blocked by nearshore heated waters (Fig. 7d). This blocking force the SACW uplift towards the surface, but it was not enough to suppress the superficial anomalous heating. Along with the Ekman transport, the

SACW uplift displaced TW towards deeper regions, as suggested by the 36 psu isohaline (Fig. 10).

The uplift mechanism was observed during a campaign in February 2014, by Aguilar (2019). The authors found more than 50% of SACW at approximately 5-m depth and sea surface temperatures higher than 27 °C, which decreases rapidly until 16 °C near the bottom. These observations corroborate the results found by numerical modeling, endorsing the cold waters uplift. Similar patterns were also observed by Dottori et al. (2015) at the São Sebastião Channel for the same period. Fig. 14 illustrates this mechanism considering a longer transect.

The southern SBB portion has a wider shelf than the northern portion, not presenting a distinguished SACW onshore advection (Castro, 1996). The lower availability of cold waters, along with the offshore Ekman transport, also displace the TW limits further offshore. However, in the subsurface, the 36 psu isohaline shows little variations in its position relative to the climatology (Fig. 10). This pattern suggests a retreat of the TW only at the surface, and it makes sense since we do not have an 18 °C-isotherm uplift in this area. Consequently, without a source of cold waters to buffer the surface heating, this region develops a warm water pool restricted to the surface. Fig. 14b illustrates this mechanism considering a longer transect.
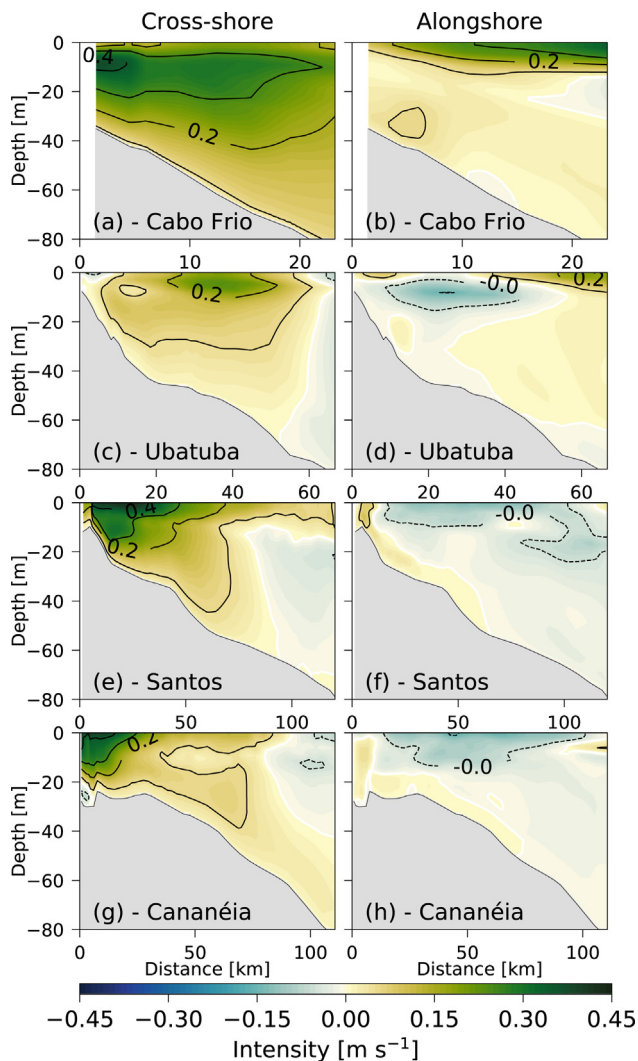
Fig. 12. Transect of cross-shore (left column) and alongshore (right column) velocity components off Cabo Frio (a and b), Ubatuba (c and d), Santos (e and f) and Cananéia (g and h) for February 13th of 2014. Positive (negative) intensity values indicate the onshore (offshore) cross-shore component and the northward (southward) alongshore component.

Due to the alongshelf cold waters transport from Cabo Frio, the Santos transect presents relatively cold waters at the surface over near the 100-m isobath (Fig. 7). This cold water contributes in reducing the solar heating at the surface, resulting in relatively moderate temperatures. Braga et al. (2017) observed a well-defined stratification during January 2014 over the 40-m isobath off Santos. In this vertical profile, they reported sea surface temperatures higher than 30 °C and temperatures lower than 16 °C near the bottom, very similar with the results shown in Fig. 7f.

The absence of cold waters off Cananéia (Fig. 7h), due to the cross or alongshelf advection, contributes to surface heating, resulting in extreme high sea surface temperatures. Rodrigues et al. (2019) describe the low latent heat flux and the high shortwave radiation, due to the lack of cloud coverage, as the leading mechanisms for the development of a large-scale marine heatwave in the southwestern Atlantic Ocean. The warm-water pool presented here might be part of this large-scale feature, with a duration of approximately 40 days, as observed in Fig. S1 of Rodrigues et al. (2019).

4.2. Hydrodynamical response

Despite the salinity homogenization near the coast, caused by a reduced continental runoff due to the drought period (Coelho et al., 2016), we observed stronger northwestward currents in the southern sector inner shelf (Fig. 11). Since this sector is highly influenced by buoyancy forces (Castro, 1996), promoting northwestward currents due to geostrophic balance (Csanady, 1997; Brink, 2005), the cross-shore SST gradient enhancement (Fig. 8) strengthened these currents. Climatologically, this pattern extends from the coast up to the 40-m isobath (Castro, 1996; Mazzini, 2009; Fontes and de Castro, 2017) but, during the 2013–2014 summer, the outer limits reached the 80-m isobath. This enlargement suppressed the typical barotropic response to the winds (Dottori and Castro, 2009). Over the 40-m isobath off Santos, Fontes and de Castro (2017) observed a similar behavior in 2014, presenting currents with preferred direction that leave the isobaths to the left in all vertical levels.

The northern sector presented a reduced horizontal density gradient due to the thermohaline homogenization (Fig. 8), weakening the alongshore component. The wind-driven response was more intense due to upwelling-favorable winds persistence during the atmospheric blocking event. However, the expected development of an Ekman cell (Lentz, 2001) was not observed on the inner and mid shelves (Fig. 12a and c), despite their development in the CE average state (not shown). This might be related to the thermal blocking. The weakening of alongshore component with stronger cross-shore components resulted in divergent currents at the surface in the northern sector (Fig. 11), transporting nearshore waters towards offshore. The mass conservation is balanced by an intensified cross-shelf onshore transport between 10-m depth and the bottom in the northern sector (Fig. 13b).

The scarcity of in situ measurements represents a major problem to investigate the influence of these events on biogeochemical water properties. Some studies have shown a negative impact of blocking episodes over the phytoplankton concentration due to high temperatures on large scales (Whitney, 2015; Le et al., 2019). Nearshore, such impacts might be positive, as Brandini et al. (2019) observed biogeochemical changes in the composition of oligotrophic waters, from the South Brazil Bight northern area, during the atmospheric blocking investigated in this work.

5. Conclusion

The 2013–2014 summer in southern South America presented anomalous climatic conditions with respect to wind, solar radiation, and a deficit in precipitation. This was due to the persistent establishment of atmospheric blocking, which deflects cold fronts eastward and suppresses SACZ formation, impacting the cloud coverage and precipitation regime. In this work, we investigate the consequences of this episode over shallow waters from a numerical perspective.

We found that enhanced shortwave radiation leads to intense surface heating and that the presence of northeasterly winds strengthens the coastal upwelling near Cabo Frio. The SACW was transported into the SBB, regulating the extreme heating in the northern half of the domain. However, without a strong source of bottom cold water, the southern half develops a warm-water pool that may be part of the marine heatwave described by Rodrigues et al. (2019) in the southwestern South Atlantic during the same period. Salinity variations, on the other hand, were not significant, but we observe a displacement of TW offshore. The final thermohaline structure induced an enlargement and intensification of the northeastward currents near the coast between Cananéia and south of São Sebastião Island. Between Ubatuba and Cabo Frio, the cross-shore component was more intense than the alongshore component due to intensified advection towards offshore, compensated with near bottom advection towards the coast.
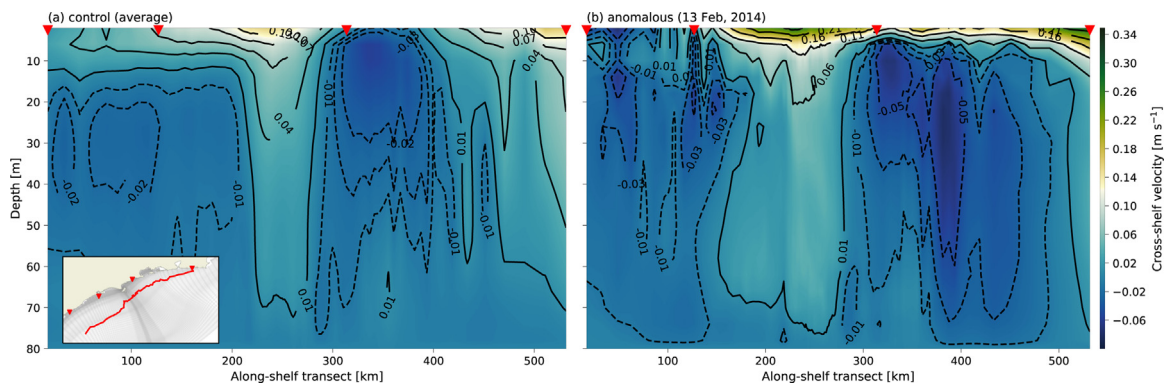
Fig. 13. Cross-shelf current component transect over the 80-m isobath, between Cananéia and Cabo Frio, for (a) the average state for CE and (b) for February 13th of 2014. Positive (negative) intensity values indicate offshore (onshore) cross-shelf component. The red triangles in both transects represents the location of cross-shelf transect used in this work, as well as the inset map highlighting this transect location.
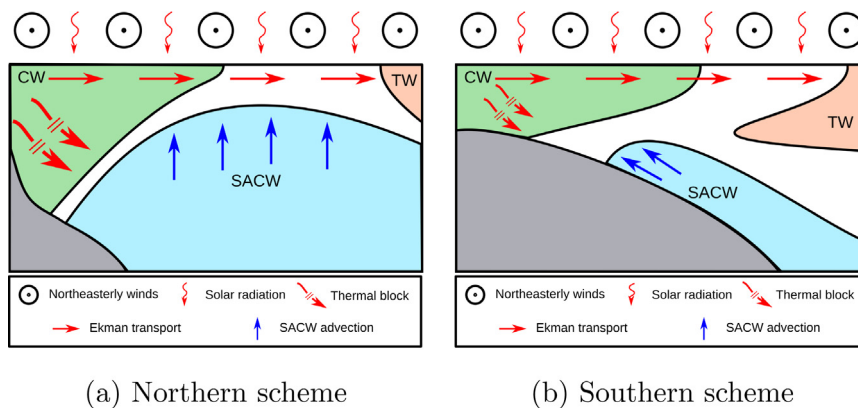
Fig. 14. Schemes that summarize the mechanisms suggested in this work, for each region of the domain, during the summer of 2014. Northern section includes Ubatuba and Cabo Frio, while the Southern section includes Cananéia and Santos. The acronyms in the images stand for South Atlantic Central Waters (SACW), Tropical Waters (TW), and Coastal Waters (CW).

CRediT authorship contribution statement

Danilo A. Silva: conceptualization, Methodology, Investigation, Software, Validation, Formal analysis, Visualization, Writing - review & editing. **Marcelo Dottori:** Resources, Conceptualization, Investigation, Supervision, Writing - review & editing.

Declaration of competing interest

The authors declare that they have no known competing financial interests or personal relationships that could have appeared to influence the work reported in this paper.

Acknowledgments

Funding information

References

Aguilar, T.I.M., 2019. Dinâmica sazonal do ictioplâncton em uma área costeira subtropical - Ubatuba, São Paulo (Ph.D. thesis). Universidade de São Paulo, São Paulo.

Beniston, M., 2004. The 2003 heat wave in Europe: A shape of things to come? An analysis based on Swiss climatological data and model simulations. Geophys. Res. Lett. 31 (2).

Berrisford, P., Hoskins, B.J., Tyrlis, E., 2007. Blocking and rossby wave breaking on the dynamical tropopause in the southern hemisphere. J. Atmos. Sci. 64 (8), 2881–2898.

Blumberg, A.F., Mellor, G.L., 1987. A description of a three-dimensional coastal ocean circulation model. In: Three-Dimensional Coastal Ocean Models, Vol. 4. pp. 1–16.

Bonetti Filho, J., de Miranda, L.B., 1997. Estimativa da descarga de água doce no sistema estuarino-lagunar de Cananéia-Iguape. Braz. J. Oceanogr. 45 (1–2), 89–94.

Brandini, F., Michelazzo, L.S., Freitas, G.R., Campos, G., Chuqui, M., Jovane, L., 2019. Carbon Flow for Plankton Metabolism of Saco do Mamanguá Ría, Bay of Ilha Grande, a Subtropical Coastal Environment in the South Brazil Bight. Front. Mar. Sci. 6.

Brink, K.H., 2005. Coastal Physical Processes Overview, Vol. 13. Harvard University Press, pp. 37–60,

Castro, B.M., 1990. Wind driven currents in the channel of São Sebastião: winter, 1979. Bol. Inst. Oceanogr. 38 (2), 111–132.

Castro, B.M., 1996. Correntes e massas deágua da plataforma continental norte de São Paulo (Ph.D. thesis). Instituto Oceanográfico da Universidade de São Paulo.

Castro, B.M., 2014. Summer/winter stratification variability in the central part of the South Brazil Bight. Cont. Shelf Res..

Castro, B.M., Miranda, L.B., 1998. Physical oceanography of the western Atlantic continental shelf located between 4 N and 34 S. The Sea 11 (1), 209–251.

Castro, B.M., Miranda, L.B., Silva, L.S., Fontes, R.F.C., Pereira, A.F., Coelho, A.L., 2008. Processos físicos: Hidrografia, circulação e transporte. In: Oceanografia de Um Ecossistema Subtropical: Plataforma de SãO SebastiãO, SP, São Paulo. EDUSP, pp. 59–121.

Cerda, C., Castro, B.M., 2014. Hydrographic climatology of South Brazil Bight shelf waters between Sao Sebastiao (24oS) and Cabo Sao Tome (22oS). Cont. Shelf Res. 89, 5–14.

Chase, T.N., Wolter, K., Pielke, R.A., Rasool, I., 2006. Was the 2003 European summer heat wave unusual in a global context? Geophys. Res. Lett. 33 (23), L23709.

Chin, T.M., Vazquez-Cuervo, J., Armstrong, E.M., 2017. A multi-scale high-resolution analysis of global sea surface temperature. Remote Sens. Environ. 200, 154–169.

Coelho, C.A.S., de Oliveira, C.P., Ambrizzi, T., Reboita, M.S., Carpenedo, C.B., Campos, J.L.P.S., Tomaziello, A.C.N., Pampuch, L.A., Custódio, M.d.S., Dutra, L.M.M., Da Rocha, R.P., Rehbein, A., 2016. The 2014 southeast Brazil austral summer drought: regional scale mechanisms and teleconnections. Clim. Dynam. 46 (11–12), 3737–3752.

Costa, C.G.R., Leite, J.R.B., Castro, B.M., Blumberg, A.F., Georgas, N., Dottori, M., Jordi, A., 2019. An operational forecasting system for physical processes in the Santos-Sao Vicente-Bertioga Estuarine System, Southeast Brazil. Ocean Dyn..

Csanady, G.T., 1997. On the theories that underlie our understanding of continental shelf circulation. J. Oceanogr. 53, 207–230.

da Silveira, I.C.A., Schmidt, A.C.K., Campos, E.J.D., de Godoi, S.S., Ikeda, Y., 2000. A corrente do Brasil ao Largo da Costa Leste brasileira (the Brazil current off the Eastern Brazilian Coast). Rev. Bras. Oceanogr 48 (2), 171–183.

Dametto, G.S., Rocha, R.P., 2006. Características climáticas dos sistemas frontais. In: Anais Do XIV Congresso Brasileiro de Meteorologia: A Meteorologia a ServiÇo Da Sociedade.

Dong, L., Mitra, C., Greer, S., Burt, E., 2018. The dynamical linkage of atmospheric blocking to drought, heatwave and urban heat island in southeastern US: A multi-scale case study. Atmosphere 9 (1).

Dottori, M., Castro, B.M., 2009. The response of the Sao Paulo continental shelf, Brazil, to synoptic winds. Ocean Dyn. 59 (4), 603–614.

Dottori, M., Castro, B.M., 2018. The role of remote wind forcing in the subinertial current variability in the central and northern parts of the South Brazil Bight. Ocean Dyn. 68 (6), 677–688.

Dottori, M., Siegle, E., Castro, B.M., 2015. Hydrodynamics and water properties at the entrance of Araçá Bay, Brazil. Ocean Dyn. 65 (12), 1731–1741.

Duchon, C.E., 1979. Lanczos filtering in one and two dimensions. J. Appl. Meteorol. 18 (8), 1016–1022.

Ebisuzaki, W., 1997. A method to estimate the statistical significance of a correlation when the data are serially correlated. J. Clim. 10 (9), 2147–2153.

Emilsson, I., 1961. The shelf and coastal waters off southern Brazil. Bul. Inst. Oceanogr. 11 (2).

Fontes, R.F.C., de Castro, B.M., 2017. Currents on the continental shelf adjacent to the Laje de Santos (SP, Brazil). Braz. J. Oceanogr. 65 (4), 595–604.

García-Herrera, R., Paredes, D., Trigo, R.M., Trigo, I.F., Hernández, E., Barriopedro, D., Mendes, M.A., 2007. The outstanding 2004/05 drought in the Iberian Peninsula: Associated atmospheric circulation. J. Hydrometeorol. 8 (3), 483–498.

Häkkinen, S., Rhines, P.B., Worthen, D.L., 2011. Atmospheric blocking and Atlantic multidecadal ocean variability. Science.

Hetland, R.D., DiMarco, S.F., 2012. Skill assessment of a hydrodynamic model of circulation over the Texas-Louisiana continental shelf. Ocean Model.

Hong, C.C., Hsu, H.H., Lin, N.H., Chiu, H., 2011. Roles of European blocking and tropical-extratropical interaction in the 2010 Pakistan flooding. Geophys. Res. Lett. 38 (13), n/a–n/a.

Ikeda, Y., 1977. Influências sazonais nas propriedades oceanográficas em grande média e pequenas escalas, de Cabo Frio-RJ a Cananéia-SP, baseadas nos dados obtidos pelo N/Oc. Wladimir Besnard (Ph.D. thesis). Universidade de São Paulo.

Josey, S.A., 2001. A comparison of ECMWF, NCEP-NCAR, and SOC surface heat fluxes with Moored Buoy measurements in the subduction region of the Northeast Atlantic. J. Clim. 14 (8), 1789.

Large, W.G., Pond, S., 1981. Open ocean momentum flux measurements in moderate to strong winds. J. Phys. Oceanogr. 11 (3), 324–336.

Le, C., Wu, S., Hu, C., Beck, M.W., Yang, X., 2019. Phytoplankton decline in the eastern North Pacific transition zone associated with atmospheric blocking. Global Change Biol. 25 (10), 3485–3493.

Lejenäs, H., 1984. Characteristics of southern hemisphere blocking as determined from a time series of observational data. Q. J. R. Meteorol. Soc. 110 (466), 967–979.

Lentz, S.J., 2001. The influence of stratification on the wind-driven cross-shelf circulation over the north carolina shelf. J. Phys. Oceanogr. 31 (9), 2749–2760.

Marengo, J.A., Nobre, C.A., Seluchi, M.E., Cuartas, A., Alves, L.M., Mendiondo, E.M., Obregón, G., Sampaio, G., 2015. A seca e a crise hídrica de 2014–2015 em São Paulo. Rev. USP (106), 31.

Mazzini, P.L.F., 2009. Correntes Subinerciais na Plataforma Continental Interna entre Peruíbe e São Sebastião: Observações (Ph.D. thesis). Universidade de São Paulo.

Mellor, G.L., Yamada, T., 1982. Development of a turbulence closure model for geophysical fluid problems. Rev. Geophys. 20 (4), 851.

Mendes, M.C.D., Trigo, R.M., Cavalcanti, I.F., DaCamara, C.C., 2008. Blocking episodes in the Southern Hemisphere: Impact on the climate of adjacent continental areas. Pure Appl. Geophys. 165 (9–10), 1941–1962.

Morais, P.H.L.S., 2016. Hidrodinâmica da Plataforma Continental Interna do estado de São Paulo (Master's thesis). Universidade de São Paulo.

Nieto-Ferreira, R., Rickenbach, T.M., Wright, E.A., 2011. The role of cold fronts in the onset of the monsoon season in the South Atlantic convergence zone. Q. J. R. Meteorol. Soc. 137 (657), 908–922.

Nobre, C.A., Marengo, J.A., Seluchi, M.E., Cuartas, A., Alves, L.M., 2016. Some characteristics and impacts of the drought and water crisis in southeastern Brazil during 2014 and 2015 some characteristics and impacts of the drought and water crisis in southeastern Brazil during 2014 and 2015. J. Water Resour. Prot. 8 (February), 252–262.

Pereira, F., Bouali, M., Polito, P.S., da Silveira, I.C.A., Candella, R.N., 2020. Discrepancies between satellite-derived and in situ SST data in the Cape Frio Upwelling System, Southeastern Brazil (23oS). Remote Sens. Lett. 11 (6), 555–562.

Pereira, A.F., Castro, B.M., Calado, L., Silveira, I.C.A., 2007. Numerical simulation of M2 internal tides in the south Brazil bight and their interaction with the Brazil current. J. Phys. Oceanogr. Oceans 112 (November 2006).

Pfahl, S., Wernli, H., 2012. Quantifying the relevance of atmospheric blocking for co-located temperature extremes in the Northern Hemisphere on (sub-)daily time scales. Geophys. Res. Lett..

Pinheiro, M.C., Ullrich, P.A., Grotjahn, R., 2019. Atmospheric blocking and inter-comparison of objective detection methods: flow field characteristics. Clim. Dynam. 53 (7–8), 4189–4216.

Reid, R.O., Bodine, B.R., 1968. Numerical model for storm surges in galveston bay. J. Waterw. Harb. Div. 94 (1), 33–58.

Rezende, J.H.M., 2003. Intrusões da água central do atlântico sul na plataforma continental sudeste durante o verã (Ph.D. thesis). Universidade de São Paulo.

Rodrigues, R.R., Taschetto, A.S., Sen Gupta, A., Foltz, G.R., 2019. Common cause for severe droughts in South America and marine heatwaves in the South Atlantic. Nat. Geosci. 12 (8), 620–626.

Rodrigues, R.R., Woollings, T., 2017. Impact of atmospheric blocking on South America in Austral Summer. J. Clim. 30 (5), 1821–1837.

Roversi, F., Rosman, P.C.C., Harari, J., 2016. Análise da renovação das águas do Sistema Estuarino de Santos usando modelagem computacional. Rev. Ambiente Água 11 (3), 566–585.

Saha, S., Moorthi, S., Pan, H., Wu, X., Wang, J., Nadiga, S., Tripp, P., Kistler, R., Woollen, J., Behringer, D., Liu, H., Stokes, D., Grumbine, R., Gayno, G., Wang, J., Hou, Y., Chuang, H., Juang, H.H., Sela, J., Iredell, M., Treadon, R., Kleist, D., Delst, P.V., Keyser, D., Derber, J., Ek, M., Meng, J., Wei, H., Yang, R., Lord, S., van den Dool, H., Kumar, A., Wang, W., Long, C., Chelliah, M., Xue, Y., Huang, B., Schemm, J., Ebisuzaki, W., Lin, R., Xie, P., Chen, M., Zhou, S., Higgins, W., Zou, C., Liu, Q., Chen, Y., Han, Y., Cucurull, L., Reynolds, R.W., Rutledge, G., Goldberg, M., 2010. NCEP climate forecast system reanalysis (CFSR) selected hourly time-series products, January 1979 to December 2010. In: Research Data Archive At the National Center for Atmospheric Research, Computational and Information Systems Laboratory. Dataset.

Saha, S., Moorthi, S., Wu, X., Wang, J., Nadiga, S., Tripp, P., Behringer, D., Hou, Y.T., Chuang, H.y., Iredell, M., Ek, M., Meng, J., Yang, R., Mendez, M.P., van den Dool, H., Zhang, Q., Wang, W., Chen, M., Becker, E., 2014. The NCEP climate forecast system version 2. J. Clim. 27 (6), 2185–2208.

Sillmann, J., Croci-Maspoli, M., 2009. Present and future atmospheric blocking and its impact on European mean and extreme climate. Geophys. Res. Lett. 36 (10), L10702.

Smagorinsky, J., 1963. General circulation experiments with the primitive equations: I. The basic experiment. Mon. Weather Rev. 91 (3), 99–164.

Stech, J.L., Lorenzzetti, J.A., De Ci@bulletncias Da Terra, D., 1992. The response of the south Brazil bight to the passage of wintertime cold fronts. J. Geophys. Res. 97 (C6), 9507–9520.

Stopa, J.E., Cheung, K.F., 2014. Intercomparison of wind and wave data from the ECMWF reanalysis interim and the NCEP climate forecast system reanalysis. Ocean Model. 75, 65–83.

Teixeira, M.S., Satyamurty, P., 2007. Dynamical and synoptic characteristics of heavy rainfall episodes in southern Brazil. Mon. Weather Rev. 135 (2), 598–617.

Tibaldi, S., Molteni, F., 2018. Atmospheric Blocking in Observation and Models, Vol. 1. pp. 1–31.

Trenberth, K.E., Mo, K.C., 1985. Blocking in the southern hemisphere. Mon. Weather Rev. 113 (1), 3–21.

Valentin, J.L., 2001. The cabo frio upwelling system, Brazil. In: Seeliger Ulrich and Kjerfve, B. (Ed.), Coastal Marine Ecosystems of Latin America. Springer Berlin Heidelberg, Berlin, Heidelberg, pp. 97–105.

Whitney, F.A., 2015. Anomalous winter winds decrease 2014 transition zone productivity in the NE Pacific. Geophys. Res. Lett. 42 (2), 428–431.

Willmott, C.J., 1981. On the validation of models. Phys. Geogr. 2 (2), 184–194.

Woollings, T., Barriopedro, D., Methven, J., Son, S.W., Martius, O., Harvey, B., Sillmann, J., Lupo, A.R., Seneviratne, S., 2018. Blocking and its response to climate change. In: Current Climate Change Reports, Vol. 4, No. 3. Springer, pp. 287–300.

Zeng, X., Zhao, M., Dickinson, R.E., 1998. Intercomparison of bulk aerodynamic algorithms for the computation of sea surface fluxes using TOGA COARE and TAO data. J. Clim. 11 (10), 2628–2644.

Zhang, X., Marta-Almeida, M., Hetland, R.D., 2012. A high-resolution pre-operational forecast model of circulation on the Texas-Louisiana continental shelf and slope. J. Oper. Oceanogr. 5 (1), 19–34.